

Journal of Materials Chemistry A

Accepted Manuscript



This article can be cited before page numbers have been issued, to do this please use: M. Manzoli, F. Vindigni, T. Tabakova, C. Lamberti, D. Dimitrov, K. Ivanov, A. Giovanni and G. Agostini, *J. Mater. Chem. A*, 2016, DOI: 10.1039/C6TA06442F.



This is an Accepted Manuscript, which has been through the Royal Society of Chemistry peer review process and has been accepted for publication.

Accepted Manuscripts are published online shortly after acceptance, before technical editing, formatting and proof reading. Using this free service, authors can make their results available to the community, in citable form, before we publish the edited article. We will replace this Accepted Manuscript with the edited and formatted Advance Article as soon as it is available.

You can find more information about Accepted Manuscripts in the [author guidelines](#).

Please note that technical editing may introduce minor changes to the text and/or graphics, which may alter content. The journal's standard [Terms & Conditions](#) and the ethical guidelines, outlined in our [author and reviewer resource centre](#), still apply. In no event shall the Royal Society of Chemistry be held responsible for any errors or omissions in this Accepted Manuscript or any consequences arising from the use of any information it contains.



Journal of Materials Chemistry A

ARTICLE

Structure-reactivity relationship in Co₃O₄ promoted Au/CeO₂ catalysts for the CH₃OH oxidation reaction revealed by *in situ* FTIR and *operando* EXAFS studies

Received 00th January 20xx,
Accepted 00th January 20xx

DOI: 10.1039/x0xx00000x

www.rsc.org/

M. Manzoli^{a*}, F. Vindigni^b, T. Tabakova^c, C. Lamberti^{b,f}, D. Dimitrov^d, K. Ivanov^d, G. Agostini^{e,g}

A strong influence of the amount of the Co₃O₄ promoter on the catalytic performance in methanol oxidation of different gold catalysts supported on ceria was observed. The activity followed the order: Au/10 wt.% Co₃O₄-doped CeO₂ > Au/5 wt.% Co₃O₄-doped CeO₂ > Au/ 15 wt.% Co₃O₄-doped CeO₂ > Au/CeO₂ > Au/Co₃O₄. FTIR measurements of adsorbed CO indicate that oxidized gold sites are initially present on the activated samples and that such species are involved in the methanol reaction. Methanol oxidation performed in static conditions gave rise at 75 °C to mainly formate species on Au/CeO₂ and to a large variety of different carbonate species on Au/10 wt.% Co₃O₄-doped CeO₂. FTIR and EXAFS analyses revealed that the active sites present on the best performing Au/CeO₂ catalyst added with 10 wt.% Co₃O₄ are oxidized gold species, close Co sites, at the interface with the support, which are reduced under reaction conditions. These species are able to activate and to react with oxygen giving rise to formate and carbonate species.

Introduction

Supported gold nanoparticles attracted significant attention due to their high catalytic activity in various oxidation reactions at low temperatures. The catalytic oxidation of Volatile Organic Compounds (VOCs), such as methanol, is a subject of considerable interest due to their relevance in many industrial applications as well as in the field of sustainable chemistry. These catalytic processes have been considered as some of the most efficient ways to reduce harmful emissions from various chemical industries. During the past two decades gold-based catalysts have been proven to be effective for many reactions of environmental significance.¹ Considerable emphasis is placed on the catalyst preparation and on the selection of the support.² The oxidation activity of gold catalysts is closely related to the size of the Au particles³ and to the ability of the support to provide active oxygen species. For this reason, the

selection of the proper support is a critical factor.

Ceria is very attractive, due to its ability to maintain high metal dispersion and to change Ce oxidation state depending on the redox conditions. The rapid change of oxidation state is related to its ability to store and release oxygen, a property measured by the "oxygen storage capacity" (OSC),⁴ which results in rapid formation and elimination of oxygen vacancy defects.⁵ These characteristics make CeO₂ a very interesting support for oxidation reactions.

In principle, the modification of ceria can increase the concentration of oxygen vacancies and a strong influence of the nature of the added oxide (Me = Fe, Mn, Sn) on the catalytic performances was observed recently by some of us.⁶ For example, it was reported that the modification of CeO₂ with different Zr amounts leads to increased catalytic activity in the CO oxidation⁷, as well as in the Water Gas Shift reaction⁸ and in the steam reforming of methanol.⁹ Moreover, gold catalysts supported on iron-modified ceria oxides containing opportune molar percentages of Fe were proved to be more active than unmodified Au/CeO₂ for total and preferential CO oxidation^{10,11} and for Water Gas Shift reaction.¹²

The beneficial influence of cobalt oxide on the CO oxidation behaviour of Au/CoO_x/CeO₂-Al₂O₃ systems was previously shown.¹³ It was found that the catalytic activity depends on the cobalt loading, which provides a submonolayer coverage of the support surface, where a CoO_x-CeO₂ interaction takes place giving rise to a synergism between Co and Ce redox properties. Indeed, Co₃O₄ itself was demonstrated to be very active in the sub-ambient CO oxidation reaction depending on the morphology and on the preferential exposition of the [1 1 0] plane in which the highest number of Co(III) sites are present.^{14,15}

^a Department of Drug Science and Technology and NIS Interdepartmental Centre, University of Torino, 10125 Torino, Italy.

^b Department of Chemistry and NIS Interdepartmental Centre, University of Torino, 10125 Torino, Italy.

^c Institute of Catalysis, Bulgarian Academy of Sciences, 1113 Sofia, Bulgaria.

^d Department of Chemistry, Agricultural University, 4000 Plovdiv, Bulgaria.

^e Leibniz Institute for Catalysis at the University of Rostock (LIKAT), Albert-Einstein-Str. 29A, D-18059 Rostock, Germany.

^f IRC "Smart Materials", Southern Federal University, Zorge Street 5, 344090 Rostov-on-Don, Russia.

^g European Synchrotron Radiation Facility, 38043 Grenoble, France.

Electronic Supplementary Information (ESI) available: [details of any supplementary information available should be included here]. See DOI: 10.1039/x0xx00000x Figures S1-S6.

ARTICLE

Journal Name

Three dimensionally ordered macroporous Au/CeO₂-Co₃O₄ catalysts showed enhanced CO preferential oxidation in H₂-rich gas mixtures¹⁶ and formaldehyde oxidation.¹⁷ The former paper proposed that the origin of the high CO conversion and CO₂ selectivity was the presence of ionic Au in intimate contact with CeO₂. In the latter one, a mechanism involving the synergistic effect between CeO₂ and Co₃O₄ supports, which greatly accelerates the surface active oxygen migration and activates the Au species was proposed to explain the improvement in the catalytic HCHO oxidation. It was established that Au/CeO₂-CoO_x catalysts prepared by mechano-chemical activation exhibited much higher activity in the reaction of complete benzene oxidation than that prepared using coprecipitation.¹⁸ The reason of this different catalytic behaviour was the existence of a Co-containing phase with enhanced redox properties that influenced both gold and modified ceria in close vicinity. Therefore, ceria supports with different amount of Co₃O₄ were prepared by mechano-chemical activation in order to optimize the content of promoter. Recently, we observed a strong influence of the nature of the added oxide on the activity of ceria-based gold catalysts for catalytic abatement of CO in waste gases.¹⁹ In particular, gold catalyst supported on ceria modified by Co₃O₄ exhibited the best performance: 100% CO conversion degree was achieved at 25 °C. The support with composition 90 wt.% CeO₂ and 10 wt.% Co₃O₄ was beneficial for the nucleation and growth of highly dispersed gold. On this system, a synergy between gold and Co-doped ceria support causes significant enhancement in the reducibility and capability for oxygen activation, which resulted in an improved oxidation activity. However, a clear correlation between the catalytic activity with the nature and structure of the active sites has not been fully established yet.

The correlation existing between catalyst structure and catalytic activity/selectivity is the main goal in research applied to catalysis.²⁰ In principle, EXAFS/XANES can give relevant complementary information on the structural and electronic properties of such systems.²¹⁻²⁵ In addition, FTIR spectroscopy represents a powerful technique to investigate the surface sites at an atomic level. In particular, the analysis of FTIR spectra of adsorbed probe molecules allows to understand the nature and the abundance of the exposed active sites as well as to have detailed information on their chemical environment.²⁶⁻³⁰ Therefore, the use of these techniques can assist in the comprehension of the parameters ruling the unique catalytic properties of gold catalysts, as well as to implement the knowledge in the design of new systems. Keeping in mind these purposes, the aim of this work was an accurate EXAFS and FTIR study on the nature of the active sites exposed at the surface of highly dispersed gold catalysts supported on ceria modified by different amounts of Co₃O₄. Research efforts were focused to achieve information on the local structure of the active sites in terms of position of cobalt atoms in respect to the gold metallic phase.

Experimental

Materials

Cerium hydroxide was synthesized by precipitation of aqueous solutions of Ce(NO₃)₃·6H₂O with K₂CO₃ at constant pH=9.0 and at a

temperature of 60 °C, aging at the same temperature for 1 hour, filtering, washing until removal of NO₃⁻ ions and drying in vacuum at 80 °C. Mixed CeO₂-Co₃O₄ supports were prepared by a simple mechano-chemical mixing procedure: a mixture of cerium hydroxide and (5, 10, 15 wt%) of laboratory-made Co₃O₄ was subjected to mechano-chemical milling for 30 min in a mortar and calcination at 400 °C for 2 hours. Hereafter the supports will be labelled as Ce5Co, Ce10Co and Ce15Co depending on cobalt oxide loading in wt%. Gold catalysts (3 ± 0.05 wt.%) were prepared by the deposition-precipitation method at constant pH 7 and temperature 60 °C. Gold was deposited on a mixed metal oxide support preliminarily suspended in water and activated in an ultrasound disintegrator under vigorous stirring. Hereafter catalysts will be labelled as AuCe5Co, AuCe10Co and AuCe15Co depending on cobalt oxide loading in wt%.

The deposition-precipitation was carried out in an automated laboratory reactor under full control of all preparation parameters (pH, temperature, stirring speed, reactant feed flow rates, etc.). After aging at 60 °C within 1 h, filtering and careful washing, the precursors were dried under vacuum at 80 °C and calcined in air at 400 °C for 2 hours. Moreover, unmodified Au/CeO₂ and Au/Co₃O₄, (hereafter labeled as AuCe and Au/Co₃O₄, respectively), used as blank samples, were also prepared by the deposition-precipitation method under the conditions described above. All initial salts used were 'analytical grade'.

Catalytic activity measurements

The catalytic activity of the samples in CH₃OH oxidation was measured using an isothermal plug flow reactor within a different temperature range. The following conditions were chosen: catalyst bed volume – 0.5 g (particle size 0.6 – 1.0 mm), inlet CH₃OH concentrations – 2.0 % balanced with air and space velocity 10000 h⁻¹. The tests were carried out by increasing the reaction temperature step-wise until complete CH₃OH oxidation. The degree of conversion was measured at every 20 °C step after stationary conversion was achieved. The behaviour was also studied during decrease of the temperature down to room temperature, again step-wise. The conversion data at increasing and decreasing temperature match well. The duration of catalytic test for each sample was about 8 hours. The reactant and product gases were analysed for methanol, CO, CO₂, O₂ and N₂ by HP 5890 Series II gas-chromatograph, equipped with flame ionization and thermal conductivity detectors and Porapak Q and MS-5A columns.

Methods

The amount of gold in all samples was analyzed by atomic absorption spectroscopy (Varian Vista MPX) and the values determined were 3 (± 0.05) wt % Au.

High resolution transmission microscopy (HRTEM) measurements were performed using a side entry Jeol JEM 3010 (300 kV) microscope equipped with a LaB₆ filament and fitted with X-ray EDS analysis by a Link ISIS 200 detector. For analyses, the powdered samples were deposited on a copper grid, coated with a porous carbon film. All digital micrographs were acquired by an Ultrascan 1000 camera and the images were processed by Gatan digital micrograph. A statistically representative number of Au particles

(i.e. 250 for each sample) was counted in order to obtain the particle size distributions.

The FTIR spectra were recorded in transmission mode at a resolution of 2.0 cm^{-1} on a Perkin-Elmer 2000 spectrometer (equipped with a MCT detector) with the samples in self-supporting pellets introduced in an AABSPEC 2000 cell allowing to run the spectra *in situ* in controlled atmosphere and temperature (from room temperature up to $600\text{ }^{\circ}\text{C}$).

As for the experiments at low temperature, the pelletised samples were introduced in a cell allowing thermal treatments in controlled atmosphere and spectrum scanning at controlled temperature (from $-180\text{ }^{\circ}\text{C}$ up to room temperature). In order to mimic the activation before the catalytic tests and to follow the effect of such activation on the nature of the exposed active sites and of the species formed during methanol oxidation reaction, the catalysts were subjected to an oxidative treatment before the measurements. The thermal treatment included heating from room temperature (r.t.) up to $200\text{ }^{\circ}\text{C}$ under outgassing below 10^{-3} mbar ; an inlet of 20 mbar of oxygen and heating up to $400\text{ }^{\circ}\text{C}$; at $400\text{ }^{\circ}\text{C}$ the oxygen was changed three times (20 mbar for 10 min each run). After that, the sample was cooled down to r.t. in oxygen and finally outgassed at the same temperature. For each spectrum, the spectrum of the sample before the inlet of the probe/reactants (CO , methanol or oxygen) or of the methanol/oxygen mixture was used as background. All reported spectra were background subtracted and normalized to the density of the pellets.

EXAFS experiments were carried out on the BM23 beamline at ESRF facility (Grenoble, France).³¹ Fluorescence XAS spectra at the Au L_{3-} edge (11.919 keV) were collected with a 13-element Ge detector. The beam energy were selected by double-crystal Si(111) monochromator, and the third harmonic rejection was performed by Rh coated mirror with an angle of -2.2 mrad .²¹ EXAFS signal were extracted and analyzed by IFEFFIT package.³² The samples were hosted inside a plug flow reactor using 1 mm quartz capillary available on BM23 for *in situ/operando* measurements.³³ The experiments can be divided into two stages. Stage 1: the samples have been heated from room temperature up to $200\text{ }^{\circ}\text{C}$ by a small furnace, then they have been treated with a mixture O_2/He ($20\text{ }\%$ $\text{O}_2\text{-He}$, $30\text{ cm}^3/\text{min}$) up to $400\text{ }^{\circ}\text{C}$. After oxygen treatment, a $\text{CO-O}_2\text{-1:1/He}$ mixture ($5\text{ }\%$ CO , $5\text{ }\%$ O_2) was fluxed at r.t.. Stage 2: the samples were heated at $200\text{ }^{\circ}\text{C}$ and treated with a mixture O_2/He ($20\text{ }\%$ $\text{O}_2\text{-He}$, $30\text{ cm}^3/\text{min}$) up to $400\text{ }^{\circ}\text{C}$. Successively the sample was cooled down to r.t. and a vapour of methanol/ O_2/He mixture ($20\text{ }\%$ $\text{O}_2\text{-He}$) was fluxed and finally the catalysts were heated up to $100\text{ }^{\circ}\text{C}$ in the reaction mixture.

Results and discussion

Catalytic activity in the CH_3OH oxidation

The temperature dependence of CH_3OH conversion degree is presented in Figure 1. The catalytic measurements indicated that the amount of promoter has a strong influence on the activity of ceria-based gold catalysts, particularly in defining the onset temperature of the catalytic activity.

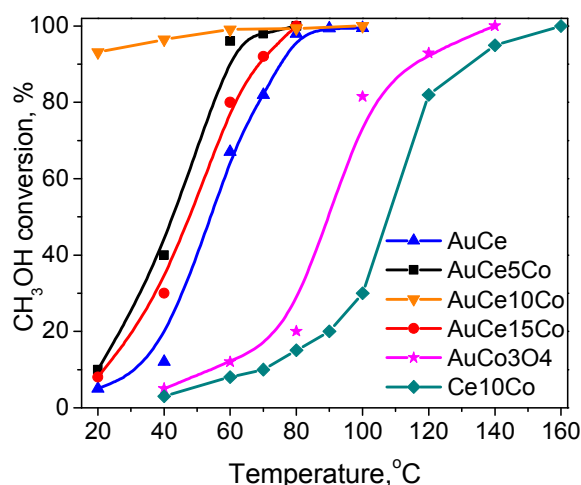


Figure 1. Temperature dependence of CH_3OH conversion over gold catalysts on ceria doped by 5, 10 and 15 wt% Co_3O_4 , over unpromoted Au/CeO_2 , $\text{Au/Co}_3\text{O}_4$ and bare ceria doped by 10 wt% Co_3O_4 .

In particular, the activity towards the CH_3OH oxidation follows the trend: $\text{AuCe10Co} > \text{AuCe5Co} > \text{AuCe15Co} > \text{AuCe} > \text{Au/Co}_3\text{O}_4 > \text{Ce10Co}$. The light-off curve related to bare ceria doped by 10 wt% Co_3O_4 appeared at the highest temperature, giving evidence of the key role displayed by gold.

The best performance was observed in the case of the catalyst doped by 10 wt% Co_3O_4 , over which almost 100% CH_3OH conversion degree at a temperature as low as $40\text{ }^{\circ}\text{C}$ was obtained. The comparison with the data recently reported by Scirè et al. (about 95 % methanol conversion at $125\text{ }^{\circ}\text{C}$ over a gold supported on ceria catalyst prepared by deposition-precipitation)³⁴ puts in evidence the promising application of AuCeO_2 catalysts doped by Co_3O_4 . Moreover, a high defectivity of ceria exposed faces, along with the presence of gold nanoparticles with the smallest size and the highest hydrogen consumption during TPR experiments (e.g. highest oxygen mobility) were found over this AuCe10Co sample, according to our previous high resolution TEM characterization.¹⁹

The light-off curves for CH_3OH oxidation of Au/CeO_2 catalysts doped by Co_3O_4 were shifted to lower temperature with respect to that of undoped Au/CeO_2 and to much lower temperature if compared to $\text{Au/Co}_3\text{O}_4$, that is also the worst catalyst. This behaviour is better pointed out from the data in Table 1, where the T_{50} conversion values (i.e. the temperature at which 50 % conversion was reached) are contrasted. From the data reported in Table 1, the promoting effect of Co_3O_4 is evident, together with the fact that the beneficial addition of cobalt oxide increases at low promoter content, reaches a maximum and then declines, in agreement with the fact that gold supported on the pure promoter phase ($\text{Au/Co}_3\text{O}_4$ sample) is the less active catalyst. In addition, it was found that the kinetic regime is not controlled by diffusional limitations. This statement is based on the experiments performed with two different catalyst pellets, the former by using a pellet with a given weight and the latter with a pellet with a double weight with respect to that employed in the first test.

ARTICLE

Table 1. Extrapolated T_{50} values for CH_3OH oxidation and calculated TOFs (s^{-1}) at two different temperatures over the catalysts.

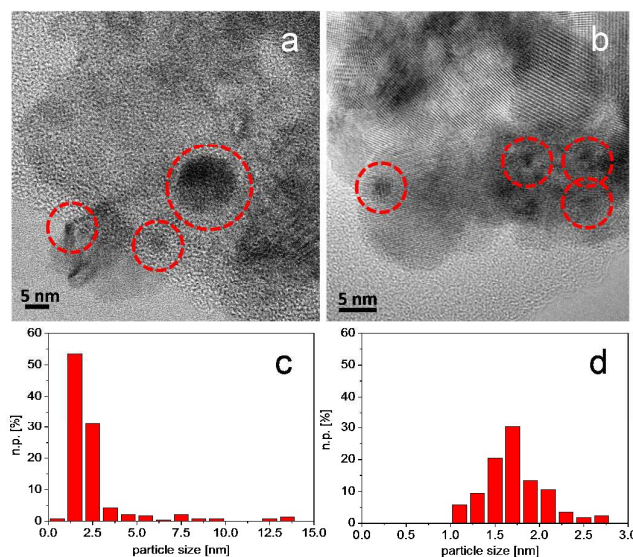
| Catalyst | CH_3OH oxidation ($^{\circ}\text{C}$) | TOF at 20 $^{\circ}\text{C}$ (s^{-1}) | TOF at 40 $^{\circ}\text{C}$ (s^{-1}) |
|-------------------|---|--|--|
| AuCeO_2 | 53 | 0.00446 | 0.0167 |
| AuCe5Co | 41 | 0.00633 | 0.0253 |
| AuCe10Co | < 20 | 0.0484 | 0.0505 |
| AuCe15Co | 47 | 0.00458 | 0.0172 |

The methanol molar flow was also doubled and a constant weight hourly space velocity was maintained at a constant partial pressure. The same methanol conversion to CO_2 in steady state regime indicated the absence of diffusion limitations. Table 1 also shows the Turnover frequencies (TOFs), expressed as s^{-1} at two different temperatures. The TOF values were calculated according to previous considerations³⁵.

Gold dispersions were calculated for all samples based on the average particle size determined by HRTEM/HAADF and reported in Ref.¹⁹ (AuCe5Co – 2.4 nm, AuCe10Co – 1.8 nm, AuCe15Co – 2.1 nm), assuming the presence of cuboctahedral particles. According to the catalytic trend for the CH_3OH conversion (see also Figure 1), the TOF values obtained for the AuCe10Co catalyst are one order of magnitude higher than those related to the other samples. The temperature has a pronounced effect on the conversion: indeed, with the exception of AuCe10Co , the obtained TOF values increase of about four times when the temperature is raised from 20 $^{\circ}\text{C}$ up to 40 $^{\circ}\text{C}$. A very recent study on Au supported on bare ceria reported the TOF values at two different temperatures.³⁶ The TOF markedly increased from $3.72 \times 10^{-5} \text{ s}^{-1}$ at 45 $^{\circ}\text{C}$ to $1.02 \times 10^{-4} \text{ s}^{-1}$ at 70 $^{\circ}\text{C}$, putting in evidence an enhancement even more accentuate, but in agreement with the data reported in Table 1. Moreover, the behaviour of AuCe5Co and AuCe15Co is very similar to the unpromoted AuCe catalyst. On the contrary, in the case of AuCe10Co , the TOF value is almost unchanged, further showing that 10 wt% Co_3O_4 provides the optimal composition for the catalysis and that for this catalyst the composition plays the major role, even with respect to the temperature.

Effect of the support composition on the gold dispersion

The catalytic activity measurements revealed almost 100% CH_3OH conversion degree at 40 $^{\circ}\text{C}$ for the AuCe10Co catalyst. Therefore, the addition of 10 wt% Co_3O_4 has improved the activity. It was previously found that the most active catalyst was that containing a big amount of Au nanoparticles with average size of 1.8 nm.¹⁹ Since the deposition-precipitation of gold was carried out on the already doped support, an evaluation of the influence of the Co_3O_4 presence on the metal dispersion and size distribution was done by performing new HRTEM measurements on the most promising AuCe10Co catalyst. The results were compared with those obtained for undoped AuCeO_2 in order to put in evidence peculiar features arisen from the different composition of the support on which the same amount of gold has been deposited. All these data are summarized in Figure 2. Both catalysts are supported on cubic CeO_2 , mainly exposing the (111) face (not shown).

**Figure 2.** HRTEM images collected on AuCeO_2 (section a) and AuCe10Co (section b), where the presence of Au nanoparticles is put in evidence by red circles. Au particle size distributions of AuCeO_2 and AuCe10Co are reported in section c and d, where n.p.= number of particles. Instrumental magnification: 300000X and 500000X, respectively.

The AuCe catalyst contains gold species with heterogeneous size in the 2–12 nm range (section a, evidenced by red circles), resulting in an average diameter equal to 7.5 ± 4.5 nm (section c). However, the particle size distribution reveals that the large majority of the roundish gold nanoparticles has size around 2 nm (more than 50%). On the contrary, the AuCe10Co catalyst exposes gold nanoparticles with smaller size (section b, evidenced by red circles), as indicated by the narrow particle size distribution, being the average size equal to 1.69 ± 0.41 nm (section d). It can be inferred that the presence of 10 wt% Co_3O_4 in the ceria support significantly affected the metal dispersion, exploiting a benefic effect in the stabilization of the Au nanoparticles during the final calcination at 400 $^{\circ}\text{C}$ and therefore favoring the formation of particles with more uniform size than in the case of AuCeO_2 . These findings are in agreement with the enhancement in the catalytic activity observed for the catalyst doped with 10 wt% Co_3O_4 .

Nature of the exposed sites and *in situ* spectra of methanol oxidation reaction

FTIR spectroscopy measurements were carried out on the bare AuCe and on AuCe10Co , i.e. on the most active doped sample. This vibrational study is aimed to investigate the effect of the promoting species on the nature and the abundance of gold exposed sites and to have information on the nature of the surface species formed during methanol oxidation from r.t. up to 100 $^{\circ}\text{C}$.

In Figure 3a, the FTIR spectra collected upon CO adsorption at r.t. on unpromoted AuCe oxidised at 400 $^{\circ}\text{C}$ are shown.

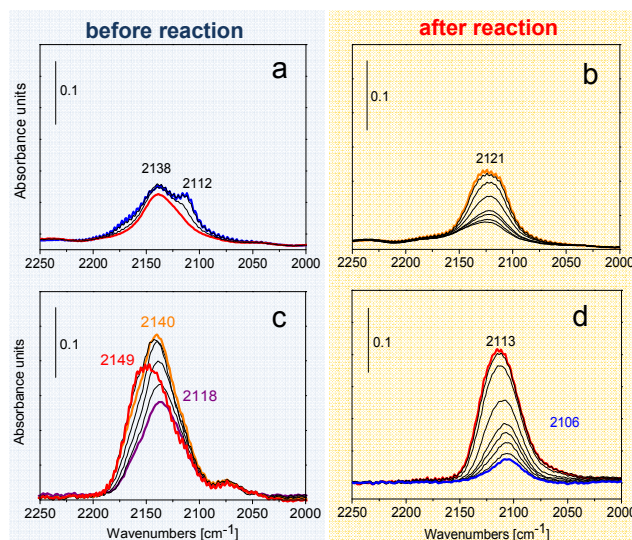


Figure 3. FTIR difference spectra collected upon CO inlet (15 mbar) at r.t. and subsequent pressure decreases down to 1.0×10^{-3} mbar on AuCe and on AuCe10Co before (sections a and c) and after (sections b and d) methanol oxidation reaction. The spectra are normalised to the density of the pellets.

Besides a shoulder at 2112 cm^{-1} , related to CO on partially oxidized metallic gold,³⁷ a broad absorption at 2138 cm^{-1} is observed after the inlet of 15 mbar CO at r.t. on AuCe (blue line). Upon CO pressure decreases at the same temperature (black lines) the band at 2138 cm^{-1} decreases in intensity without changing position, whilst the shoulder at lower wavenumber is totally depleted. The residual absorption is irreversible to the outgassing at r.t. (down to 1.0×10^{-3} mbar, red line), giving an anomalous evidence of a strong bond between CO and the involved adsorption sites, since CO is usually reversibly adsorbed on metallic gold. Some of us reported on a similar band some years ago and assigned it to CO on positively charged Au_n^+ clusters, where $4 \leq n \leq 6$ stabilized on the oxidized surface of ceria.³⁸ This assignment was supported by DFT calculations of Wu et al.³⁹, showing that the adsorption energy of CO on small cationic, neutral, and anionic clusters progressively increases with the electron depletion from the cluster. Also the calculated C-O stretching frequencies supported this assignment as they increased with increasing the positive charge on the clusters. In addition, also the paper by Fielicke et al.⁴⁰ in which the CO vibrational frequencies of $\text{Au}_n(\text{CO})_m^+$ complexes in the gas phase ($3 \leq n \leq 10$ and $3 \leq m \leq 8$) have been measured experimentally, corroborated our assignment together with further spectroscopic findings. Cationic gold clusters are still present after methanol oxidation reaction, as signalled by the broad band at 2121 cm^{-1} , whilst no bands related to oxidised gold species exposed at the surface of the nanoparticles have been detected (Figure 3b). The inlet of the CO probe at r.t. on the AuCe10Co catalyst (Figure 3c) produced a band at 2149 cm^{-1} (red line) that despite the decrease of the CO pressure, firstly increases in intensity and red shifts at 2140 cm^{-1} (orange line) and then decreases in intensity and moves to 2135 cm^{-1} (black lines down to violet line). Also in this case the residual absorption is irreversible to the outgassing at r.t. (violet

line). These results indicate the absence of partially oxidized metallic gold (band at 2112 cm^{-1})³⁰, showing that only cationic gold clusters with the same nuclearity as those detected on AuCe are exposed at the surface of the oxidised AuCe10Co sample before reaction. Moreover, if the spectra are compared with those reported in section a, the amount of these species is higher on the Co-containing sample. The increased intensity of this absorption despite the reduction of the CO pressure is an indication that the small cationic gold clusters are initially covered by adsorbed oxygen and probably are in a higher oxidized state. Indeed, the inlet of the probe at r.t. produced some CO_2 by reaction of CO and oxygen adsorbed on gold clusters and big amounts of mono-, bi- and polydentate carbonate species are observed (see Figure S1). On the contrary, only oxidised gold species exposed at the surface of the nanoparticles are observed after methanol oxidation reaction, as indicated by the presence of a band centred at 2113 cm^{-1} (Figure 3d). It is worth noting that no CO is adsorbed at r.t. on the Ce10Co sample, indicating that neither cerium nor cobalt cations are able to adsorb the probe in our experimental conditions. However, previous experiments carried out at low temperature demonstrated the presence of Ce^{4+} at the surface of both samples. Interestingly, the presence of bands related to Co^{3+} cations was hardly hypothesized on AuCe10Co.¹⁹

The AuCe and AuCe10Co catalysts were contacted with methanol (5 mbar) and then oxygen (5 mbar) at r.t. and then the temperature was gradually increased up to 100°C in order to follow the formation (and the possible evolution) of surface species during methanol oxidation by *in situ* FTIR spectroscopy. Notwithstanding that *in situ* conditions, under static equilibrium pressure of the reactants are far away from the ideal *operando* conditions where reactants are sent in a plug-flow reactor, FTIR spectroscopy can provide insights on both spectators and intermediate species formed on the different catalysts. Firstly, the inlet of methanol at r.t. on AuCe and AuCe10Co (blue lines in Figure S2) produced different amounts of on top, doubly (two species) and triply bridged methoxy species, as summarised in Table 2, where the vibrations related to the methoxy species adsorbed on AuCe and on AuCe10Co catalysts are reported. The evolution of the methoxy species at increasing temperature is shown in Figure S2 (from brown to red lines). On top and different doubly bridged methoxy species have been detected on both samples^{41, 42}, starting from room temperature (blue line) up to 50°C (brown lines), then a marked increase in intensity of the bands related to on top methoxy species is observed at 75°C (violet lines). Methoxy species are definitely more abundant on AuCe10Co than on AuCe, in particular the intensity of the absorptions due to the doubly bridged methoxy species with different coordination of Ce cations with oxygen ions (bands at 1053 and 1038 cm^{-1}) seems enhanced on AuCe10Co, further indicating that the addition of cobalt leads to a lower degree of coordination of the ceria surface sites of the doped sample and as a consequence to an enhanced reactivity towards the same amount of methanol. It has been reported that methoxy species formed upon methanol dissociation over CeO_2 behave both as spectators and intermediate species, depending on their proximity with gold nanoparticles.³⁶ It can be proposed that on AuCe10Co, that is the most active catalyst, the higher is the metal

ARTICLE

dispersion, the larger is the amount of active methoxy species acting as reaction intermediates.

The above findings are also in agreement with the results of the previous analysis of the HRTEM diffraction fringes related to the ceria-containing phases, indicating an increase of about four times of the spacings due to defective ceria phases for AuCe10Co (37.35%) if compared to AuCe (10.77 %).¹⁹

The presence of more defective ceria may also favour the formation of double bridged reactive methoxy species on the surface of the catalyst. In addition, triply bridged methoxy species are easily distinguishable on AuCe10Co also at 100 °C,^{25, 26} whilst they are almost depleted at the same temperature on AuCe, as indicated by the weak bands at 1026, 2847 and 2934 cm⁻¹. These features further indicate that, due to the presence of cobalt, AuCe10Co displays a more easy activation of methanol and an enhanced reactivity of methoxy species if compared to AuCe.

The FTIR spectra collected on AuCe and on AuCe10Co in contact with the methanol/oxygen mixture at increasing temperature are reported in Figure 4 section a and b, respectively.

On the AuCe sample, the methanol oxidation was mainly limited to the production of bidentate (bands at 2845, 1572, 1549, 1398, 1371 cm⁻¹) and monodentate (bands at 1605 and 1250 cm⁻¹) formate species.⁴³ However, bands related to monodentate (1507 and 1358 cm⁻¹), bidentate (1564, 1299, 1022, 856 cm⁻¹) and polydentate (1475, 1053 and 833 cm⁻¹) carbonate species²⁷ start to increase in intensity at 75 °C, simultaneously with the decrease of the bands related to methoxy species (see Figure 5 and Figure S2, where the methoxy region in the 1150–950 cm⁻¹ region is zoomed).

The FTIR results put in evidence that on both catalysts methanol reacted with the surface giving rise to different methoxy species at r.t. and to formates at 50 °C. These species further evolved to mono-, bi- and polydentate carbonates by increasing the temperature at 75 °C and up to 100°C. On AuCe10Co larger amounts of carbonates are produced.

Table 2. Wavenumbers for vibrations of on top, doubly (two species) and triply bridged methoxy species adsorbed on AuCe and on AuCe10Co catalysts.

| Vibrational modes | $\nu_a(\text{CH}_3)$ cm ⁻¹ | $2\delta(\text{CH}_3)$ cm ⁻¹ | $\nu_s(\text{CH}_3)$ cm ⁻¹ | $\nu(\text{OC})$ cm ⁻¹ |
|--|--|--|--|--------------------------------------|
| <i>On top methoxy species</i> | | | | |
| AuCe | 2911 | 2884 | 2801 | 1105 |
| AuCe10Co | 2911 | 2881 | 2800 | 1105 |
| <i>Doubly bridged methoxy species</i> | | | | |
| AuCe | 2923 | 2834 | 2800 | 1050 |
| AuCe10Co | 2936 | 2838 | 2801 | 1053 |
| <i>Doubly bridged methoxy species with different coordination of Ce cations with oxygen ions</i> | | | | |
| AuCe | 2910 | 2841 | 2807 | 1039 |
| AuCe10Co | 2911 | 2838 | 2809 | 1038 |
| <i>Triply bridged methoxy species</i> | | | | |
| AuCe | 2934 | 2847 | - | 1026 |
| AuCe10Co | 2949 | 2836 | - | 1023 |

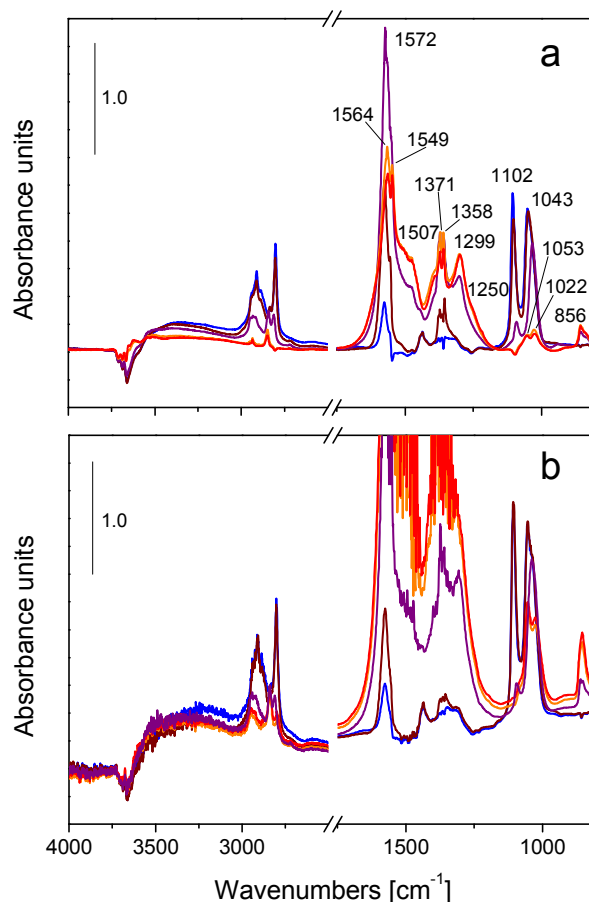


Figure 4. FTIR difference spectra collected on AuCe (section a) and AuCe10Co (section b) in contact with the methanol/oxygen mixture after 10 min at r.t. (blue lines), at 50 °C (brown lines), 75 °C (violet lines), at 100 °C (orange lines) and after 20 min (red lines) at the same temperature.

Differently from what previously observed in a combined steady state isotopic transient kinetic analysis and *operando* FTIR study³⁶, bands related to the presence of carbonate species were also detected due to the adopted experimental conditions (static conditions rather than flow conditions reported in the literature³⁶). The presence of carbonates indicates that formate species are converted into CO₂, that evolves into surface carbonates in static conditions, whereas they would be flushed away in dynamic flow. The comparison between *in situ* and *operando*³⁶ experiments indicates that both methoxy and formate species are intermediates and not simply spectators.

The thermal methanol decomposition was also performed on both catalysts in order to compare the results with experiments carried out without oxygen: it was observed that on AuCe on top methoxy species disappeared along with the formation of formate species at 100°C, simultaneously to the conversion of doubly bridged methoxy with different coordination into more coordinated doubly bridged methoxy species (Figure S3). Therefore, the methoxy species with different coordinative unsaturation could be related to the formate

production. On the contrary, in the case of AuCe10Co no formate species have been observed and only very intense bands due to carbonate-like species are produced (Figure S4), whereas the behaviour of the methoxy species is the same as observed on AuCe for the same reaction. These results demonstrate that in the absence of oxygen as a reactant, the AuCe10Co catalyst is able to efficiently provide oxygen to decompose methanol, further confirming that on this system the addition of Co causes a significant enhancement in the reducibility, which resulted in an improved oxidation activity.¹⁸ However, the same reaction carried out on the bare Ce10Co support did not give rise to any product (Figure S5) indicating that there must be a positive synergy involving gold to enhance oxygen mobility and activation.

It has been reported that promoting supported gold nanoparticles with lanthanum oxide largely increases the hydrogen selectivity in the partial oxidation of methanol, due to the fact that La_2O_3 was found to facilitate the reduction of initially present oxidic gold species.⁴⁴ If compared with the results related to AuCe, the CO adsorption experiments at room temperature revealed the presence of more positivized gold sites on AuCe10Co before methanol oxidation reaction (Figure 3c). These sites could be responsible of the enhanced reactivity displayed by AuCe10Co and appear also to be reduced in higher extent after reaction (Figure 3d), demonstrating that an effect of the addition of cobalt on gold is occurring.

Insights on the structure of the active sites

In order to investigate the effect of the Co addition to the ceria substrate on the average local environment of supported gold (5, 10 and 15 wt.%) Au L_3 edge EXAFS experiments were performed on the AuCe, AuCe5Co, AuCe10Co and AuCe15Co catalysts previously submitted to a thermal treatment in O_2 at 400°C, that is the activation procedure to which the catalyst underwent before the catalytic tests.

The k^3 -weighted, phase uncorrected, FT of the EXAFS spectra collected on all catalysts are shown in Figure 5, section a. The analogous spectrum collected on Au foil is also reported for comparison (grey line).

All spectra are characterized by two main contributions. The first one, appearing in the 1.0-2.0 Å region and having a maximum at about 1.55 Å, is due to the single scattering Au-O of an Au oxide phase. The second one contributes in the 2.0-3.5 Å region and, independently from the presence of two maxima at 2.39, 2.98 Å, is mainly due to the first shell single scattering Au-Au of supported metal nanoparticles.⁴⁵ This assignment is supported by the imaginary parts of the FT (see Figure S6). Moreover, the AuCe10Co catalyst shows the highest intensity of Au-O component due to the interaction between the active gold nanoparticles and the oxygen atoms of the oxidic support. This EXAFS evidence is in accordance with the FTIR characterization results here discussed and with previous high angle annular dark field observations that revealed the smallest average size of gold particles on this catalyst if compared to AuCe5Co and AuCe15Co.^{19, 46}

The quantitative results obtained from the EXAFS fits on all the samples are summarized in Table 3.

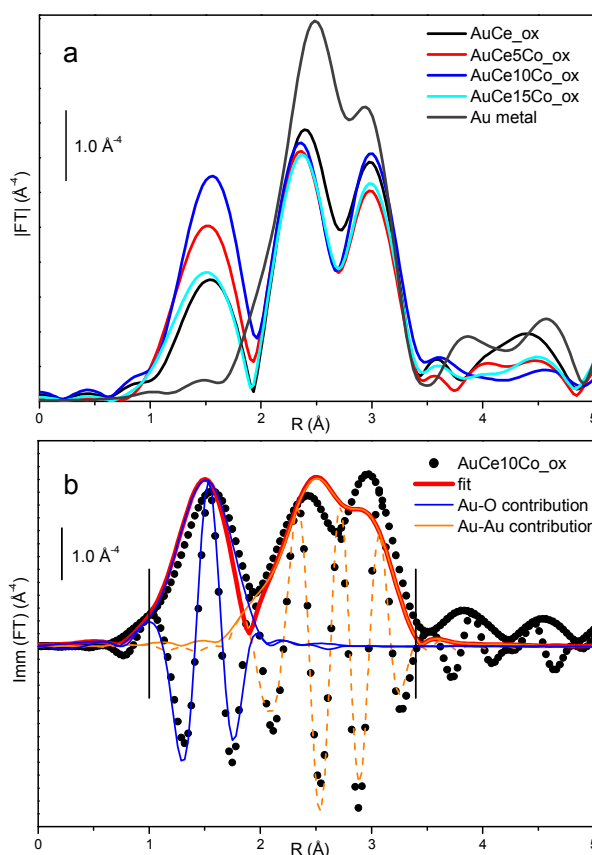


Figure 5. Section (a): modulus of k^3 -weighted, phase uncorrected, FT of the Au L_3 -edge EXAFS spectra of the catalysts prepared on differently Co doped ceria substrate and submitted to thermal treatment in oxygen at 400°C. Corresponding imaginary parts are reported in Figure S5. Section (b): Comparison between the experimental (scattered black dots) and the best fit (red full line) for AuCe10Co_ox. Also reported are the imaginary parts of the experimental data (scattered black dots) and the modulus (full lines) and the imaginary parts (dashed lines) of the individual Au-O (blue lines) and Au-Au (orange lines) contributions.

The quantitative results confirm what observed previously on the simple basis of the intensity of the Au-O component at 1.55 Å: the sample with the highest oxidized fraction is AuCe10Co, followed by AuCe5Co and then by AuCe15Co, that is comparable with the undoped AuCe. Conversely, no trend can be put in evidence for the Au-Au contributions that are formally equivalent within the experimental error bars. It should be noted that in this case the intensity of the Au-Au contribution is inversely proportional to the fraction of the oxidized phase discussed above but is also influenced by the different particle size distribution,^{47, 48} so that the two effect cannot be directly disentangled in a straightforward manner. On top of these the region between 2.0-3.5 Å is expected to host also the higher shell contributions from oxide phase, that have been neglected in these refinements. This fact also explains the minor discrepancy between experimental data and fit reported in Figure 5b.

ARTICLE

Journal Name

The methanol oxidation reaction was then investigated on Au10CoCe sample, being the most active catalyst: the first set of spectra was collected at room temperature. Furthermore, starting from the catalysts previously oxidized, another set of spectra was recorded under *operando* conditions, flowing methanol and oxygen, starting from room up to 120 °C. Au/CeO₂ was measured as reference sample, too. Three subsequent $\chi(k)$ spectra were measured at each temperature, to evaluate the experimental uncertainty.⁴⁹ The data analysis was performed on the averaged $\chi(k)$ spectrum by non-linear fitting procedures. Figure 6 shows the k^3 weighted, phase uncorrected FT (module and imaginary part) of the AuCe10Co sample collected during methanol oxidation reaction at 120 °C (black scattered points). The signal due to the Au-O distance at 1.55 Å disappears during reaction⁵⁰ while, a new contribution at about 1.8 Å is observed. The component at high distances (2.0-3.5 Å range) is clearly due to Au-Au contributions, whereas the new component around 1.8 Å is associated to an Au-Co contribution. The EXAFS fit of the experimental data performed assuming such structural model (red line in Figure 6) clearly shows the good agreement with the experimental spectrum, validating the presence of Co in the first coordination shell of a fraction of Au atoms. The quantitative results of the fit are reported in Table 4. The EXAFS study, corroborated by FTIR measurements, performed on all catalysts indicate that oxidized gold species are involved in the methanol reaction (Figure 5 and related data analysis in Table 3). In addition, the EXAFS analysis of the catalyst in working condition (Figure 6) suggests that the active sites present on the most active sample (with 10 wt% Co₂O₃) are those where gold sites are strongly interacting with Co. On these active sites reactive oxygen species, possibly close to Co sites can be activated and participate to the oxidative dehydrogenation reaction of methanol to formate species³⁶. Moreover, due to the synergic effect between cobalt and gold, the AuCe10Co catalyst is also able to provide reactive oxygen species in reaction conditions: reduced gold species close to oxygen vacancies and in strong interaction with cobalt ions are formed after reaction. Such Au species are those located at the interface with the support. These features can be at the origin of the enhanced catalytic activity of AuCe10Co.

Promotional role of Co on oxygen mobility

Spectroscopic evidence of the effect of the support composition on the oxygen mobility is reported in Figure 7, where the evolution of

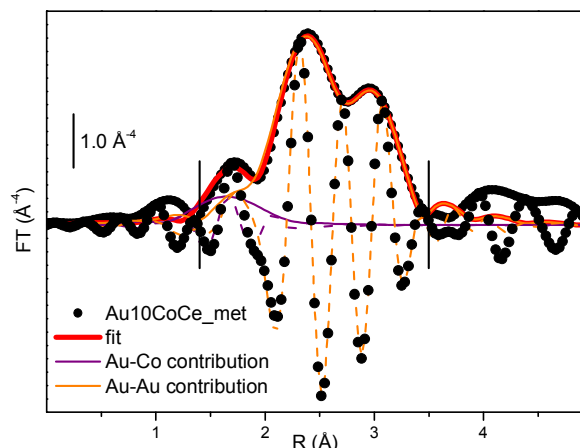


Figure 6. Modulus of the k^3 -weighted, phase uncorrected, FT of the Au L₃-edge EXAFS spectrum of AuCe10Co collected during methanol oxidation reaction at 120 °C (black scattered dots) compared with the fit (red curve). Also reported are the imaginary parts of the experimental data (black scattered dots) and the modulus (full lines) and the imaginary parts (dashed lines) of the individual Au-Co (purple lines) and Au-Au (orange lines) contributions.

the bands during CO and ¹⁸O₂ interaction on all the samples is shown starting from -180 °C (orange lines, i.e. immediately after the inlet of ¹⁸O₂ on preadsorbed CO), during the heating (black and purple lines) and up to room temperature (blue lines).

Table 4. Result of the fit performed on AuCe10Co_{met} EXAFS spectrum.

| | CN | σ^2 (Å ²) | R (Å) | E ₀ (eV) |
|---------|---------|------------------------------|-------------|---------------------|
| Paths | | Å ⁻² | Å | eV |
| Au – Co | 0.3±0.1 | 0.010±0.001 | 2.09±0.03 | 3.6±0.7 |
| Au – Au | 8.8±0.8 | | 2.835±0.007 | |

$S_0^2 = 0.85$ fixed from the value extracted from the fit of the Au foil ($S_0^2 = 0.85 \pm 0.8$); $\Delta k = (3.3-10.0)$ Å⁻¹ and $\Delta R = (1.4-3.5)$ Å, resulting in a number of independent points larger than 11; R factor = 0.005.

Table 3. Results of the fit performed on oxidized samples.

| | CN | | σ^2 (Å ²) | | R (Å) | | E ₀ (eV) | r factor |
|----------|---------|---------|------------------------------|-------------|-----------|-------------|---------------------|----------|
| | Au – O | Au – Au | Au – O | Au – Au | Au – O | Au – Au | | |
| AuCe | 1.2±0.3 | 5.5±1.1 | 0.006±0.001 | 0.004±0.002 | 1.96±0.02 | 2.854±0.012 | 5.3±2.2 | 0.002 |
| AuCe5Co | 1.7±0.3 | 4.6±0.5 | | | 1.95±0.01 | 2.848±0.006 | | 0.006 |
| AuCe10Co | 2.2±0.4 | 5.0±0.6 | | | 1.94±0.02 | 2.852±0.008 | | 0.010 |
| AuCe15Co | 1.2±0.2 | 4.7±0.3 | | | 1.95±0.01 | 2.850±0.004 | | 0.003 |

$S_0^2 = 0.85$ fixed from the value extracted from the fit of the Au foil ($S_0^2 = 0.85 \pm 0.8$); $\Delta k = (3.3-10.0)$ Å⁻¹ and $\Delta R = (1.4-3.5)$ Å, resulting in a number of independent points larger than 11.

Journal of Materials Chemistry A

ARTICLE

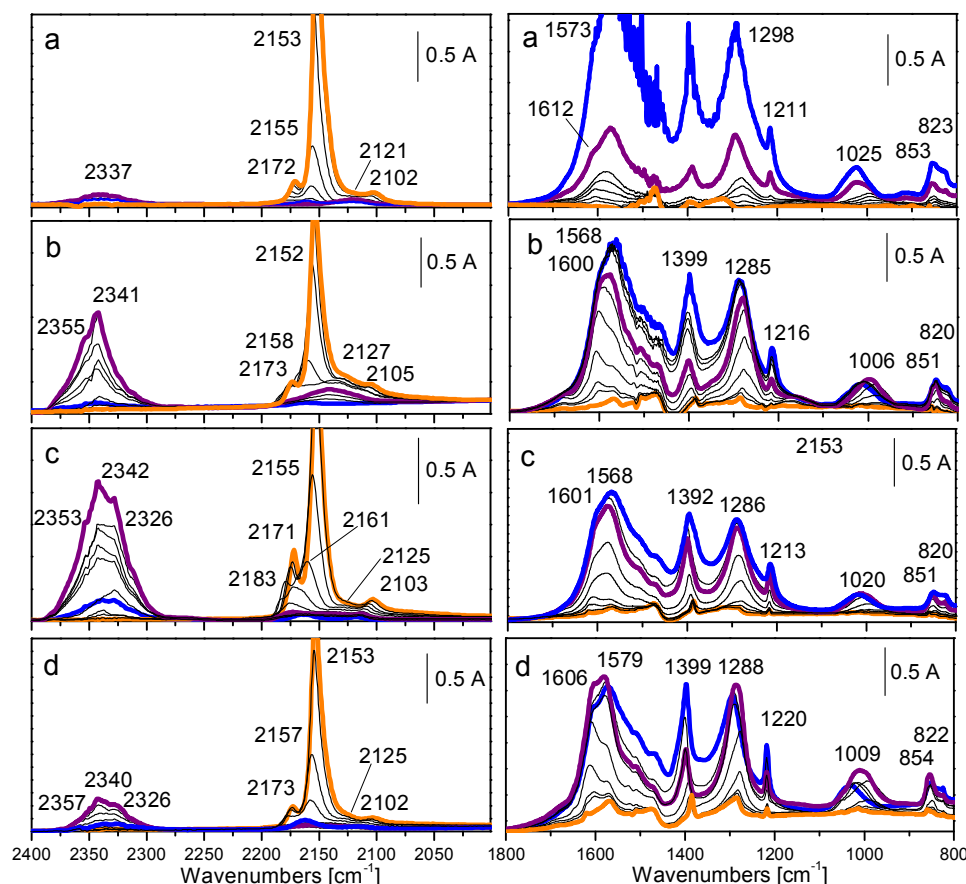


Figure 7. Evolution of FTIR difference spectra collected on AuCe (section a), AuCe5Co (section b), AuCe10Co (section c) and AuCe15Co (section d) oxidised at 400 °C immediately after the inlet of $^{18}\text{O}_2$ at -180 °C on preadsorbed CO (orange lines) and at increasing contact times and temperature (black and purple lines) up to room temperature (blue lines) in the 2000-2400 cm^{-1} (left) and in the 1800-800 cm^{-1} (right) regions. The spectrum collected before CO dosage has been used to obtain the reported difference spectra, that have been normalised to the density of the pellets.

The inlet of $^{18}\text{O}_2$ at increasing diffusion times and temperature (black and purple lines up to blue line) over the samples previously saturated by CO at -180 °C (orange line) caused an erosion from the low-frequency side of the band at about 2102-2105 cm^{-1} , due to CO on Au particles covered by adsorbed oxygen³⁷, a gradual decrease in intensity of the component at 2121-2127 cm^{-1} due to CO adsorbed on cationic gold clusters³⁸⁻⁴⁰ and the rapid depletion of the bands related to the support (component at 2150 cm^{-1} due to CO in interaction OH groups and bands at 2155-2161 cm^{-1} and at 2171-2173 cm^{-1} due to CO on different Ce^{4+} sites⁴³). Only in the case of AuCe10Co a band at 2183 cm^{-1} , tentatively assigned to CO adsorbed on Co^{x+} sites⁵¹ is observed during the heating at room

temperature. Simultaneously, bands related to CO_2 formation during CO oxidation are produced at higher frequencies (asymmetric CO_2 stretching or ν_3 mode⁵²). Such absorptions have the highest intensity in the case of AuCe10Co (section c) and their intensity follows the same trend as for the catalytic activity: AuCe10Co > AuCe5Co > AuCe15Co > AuCe. More in detail, the three isotopomers of the CO_2 molecule were observed: a growing band at 2326 cm^{-1} , assigned to the $\text{C}^{16}\text{O}^{18}\text{O}$ solid-like phase, accompanied by bands at 2340-2342 and at 2353-2357 cm^{-1} , assigned to C^{16}O_2 and C^{18}O_2 solid-like phase, respectively⁵³. The spectra showed that a rapid exchange between the oxygen of ceria and the $^{18}\text{O}_2$ molecules coming from the gas phase occurred already at low temperature.

Moreover, the high intensity of the band ascribed to $C^{16}O_2$ indicated that oxygen participating in the reaction at low temperature mainly comes from the support, putting in evidence the fact that the catalyst promotion with Co led to increased oxygen mobility because of the improved exchange properties of the ceria support. The results demonstrated the enhanced ability of the Co-promoted-ceria support to supply active lattice oxygen that is beneficial for the reaction and were in good agreement with already published TPR results¹⁷ for highest hydrogen consumption and shift of T_{max} to lower temperature observed in the profile of AuCe10Co sample. Here we recall that these experiments were performed on catalysts oxidised at 400 °C, i.e. the temperature used for the activation before performing the catalytic tests on CH_3OH oxidation, see Figure 1, Table 1 and related discussion.

On the stability of the catalysts

The analysis of the spectra reported in Figure 7 (right) indicated that on all the samples mainly two kinds of carbonate-like species were formed simultaneously to the production of CO_2 (see the spectra reported in the right parts of Figure 7). Such species have different abundance, depending on the composition of the four catalysts. Hydrogen carbonates with peaks at 1600-1612 cm^{-1} , 1392-1399 cm^{-1} and the component around 1020 cm^{-1} (νCO_3 modes), at 820-823 cm^{-1} (πCO_3) and at 1211-1220 cm^{-1} (δOH) were detected.⁴³ In addition, bidentate carbonates are also produced, as revealed by the absorptions at 1568-1579 cm^{-1} , at 1285-1298 cm^{-1} and at 1006-1009 cm^{-1} (νCO_3 modes) and at 851-854 cm^{-1} (πCO_3).⁴³ Please note that approximatively in the 1350-1400 cm^{-1} region there must be the symmetric CO_2 stretching (or ν_1 mode) of the CO_2 molecules giving rise to the ν_3 mode (complex band at 2320-2360 cm^{-1} discussed above). For symmetry reason this band is IR inactive for CO_2 molecules in the gas phase, but becomes IR active upon surface adsorption because of symmetry break. However, as the absorption coefficient of the ν_1 mode of adsorbed CO_2 is typically one order of magnitude lower than that of the ν_3 mode⁵², meaning that we can neglect their presence in the spectra reported in the right parts of Figure 7.

Summarizing this isotopically labelled IR study, it is found that the presence of another oxide to ceria has a remarkable influence on the intensity of the bands in the carbonate region: on the AuCe catalyst (section a) the highest amount of hydrogen carbonate as well as of bidentate carbonate species is adsorbed on the surface after reaction if compared to the Co-promoted catalysts. Indeed, the intensity of such bands decreases with increasing the amount of produced CO_2 , giving evidence that cobalt oxide lowers the basicity of ceria and therefore the carbonate species formation results inhibited, despite the CO_2 formation. AuCe10Co is the most active catalyst, but also the most stable one, due to the highest amount of produced CO_2 and the lowest amount of carbonate-like species present at the surface after reaction. This represents a remarkable achievement for the promotion of the gold on ceria catalyst with Co, as in most of the cases in catalysis an increase of the catalyst activity is accompanied by a faster deactivation time and compromises must be found about these two aspects of the promotion.

Conclusions

The catalytic performance in methanol oxidation of different gold catalysts supported on ceria modified by the addition of Co_3O_4 was investigated. Au/CeO₂ and Au/Co₃O₄ were also studied as reference

samples. A strong influence of the amount of the Co promoter was observed. The activity trend followed the order: AuCe10Co > AuCe5Co > AuCe15Co > AuCe >> Au/Co₃O₄. TOFs have been calculated for all catalysts, and it was found that the TOF values obtained for AuCe10Co are one order of magnitude higher than those related to the other catalysts. Moreover, with the exception of AuCe10Co, for which the TOF value is almost unchanged, the conversion is strongly dependent on the temperature.

Different *in situ* FTIR experiments were performed. Adsorption of CO on AuCe and AuCe10Co indicate that oxidized gold sites are initially present on both activated samples, suggesting that such species are involved in the methanol reaction. Upon CH_3OH dosage, different methoxy groups are formed on both catalysts at r.t. (more abundantly on AuCe10Co). After successive O_2 addition they are consumed on both catalysts starting at about 75 °C and giving rise to mainly formate species on AuCe and to big amounts of different carbonate species on AuCe10Co. Moreover, the synergy between gold and Co-promoted ceria support causes significant enhancement of reducibility and capability for oxygen activation, which resulted in an improved oxidation activity, as demonstrated by the FTIR experiments carried out in the absence of oxygen. The capability of AuCe10Co to supply active oxygen species involves the participation of the oxygen vacancies on modified ceria as well as of the surface of separate, highly reducible, CoO_x phase.

As suggested by EXAFS analyses, the active sites present on the best performing AuCe10Co catalyst are oxidized gold species at the interface with the support and close to Co sites, which are able to activate and to react with oxygen giving rise to the formation of formate species and of carbonate species. The presence of a multiplet of bands in the CO_2 asymmetric stretching region after CO interaction with $^{18}O_2$ clearly reveals that the promotion of ceria by Co facilitates the exchange reaction with the $^{16}O_2$ atoms of the support. Moreover, it is demonstrated that the production of carbonate species is lowered in the presence of cobalt oxide, despite the CO_2 formation is increased. Such results give evidence of an improved stability of the Co-promoted catalysts.

The correlation of the catalytic activity and of a well-defined metal dispersion with the findings, provided by *in situ* FTIR and *operando* EXAFS studies about the nature and structure of the active sites allows to bridge the gap of experimental data previously obtained by HAADF, XRD, FTIR, TPR and to clarify the precise nature of the synergy between the gold phase and the Co-promoted ceria support, which resulted in an excellent CH_3OH oxidation activity.

Acknowledgements

M. Manzoli and F. Vindigni gratefully acknowledge the IIT (Istituto Italiano di Tecnologia) for financial support (NANO GOLD Project). The Bulgarian authors gratefully acknowledge the financial support by the Bulgarian National Science Fund (Project DFNI T 02/4). C. Lamberti acknowledges the Mega-grant of the Russian Federation Government to support scientific research at the Southern Federal University, no. 14.Y26.31.0001.

References

1. S. Scire and L. F. Liotta, *Appl. Catal. B-Env.*, 2012, **125**, 222-246.

2. T. Tabakova, G. Avgouropoulos, J. Papavasiliou, M. Manzoli, F. Boccuzzi, K. Tenchev, F. Vindigni and T. Ioannides, *Appl. Catal. B: Env.*, 2011, **101**, 256-265.
3. A. Taketoshi and M. Haruta, *Chem. Lett.*, 2014, **43**, 380-387.
4. M. Melchionna and P. Fornasiero, *Materials Today*, 2014, **17**, 349-357.
5. P. Dutta, S. Pal, M. S. Seehra, Y. Shi, E. M. Eyring and R. D. Ernst, *Chem. Mater.*, 2006, **18**, 5144-5146.
6. T. Tabakova, L. Ilieva, I. Ivanov, R. Zanella, J. W. Sobczak, W. Lisowski, Z. Kaszkur and D. Andreeva, *Appl. Catal. B-Env.*, 2013, **136**, 70-80.
7. O. H. Laguna, A. Perez, M. A. Centeno and J. A. Odriozola, *Appl. Catal. B-Env.*, 2015, **176**, 385-395.
8. F. Vindigni, M. Manzoli, T. Tabakova, V. Idakiev, F. Boccuzzi and A. Chiorino, *Appl. Catal. B-Env.*, 2012, **125**, 507-515.
9. C. Pojanavaraphan, A. Luengnarumitchai and E. Gulari, *Int. J. Hydrogen Energy*, 2013, **38**, 1348-1362.
10. O. H. Laguna, M. A. Centeno, G. Arzamendi, L. M. Gandia, F. Romero-Sarria and J. A. Odriozola, *Catal. Today*, 2010, **157**, 155-159.
11. L. Ilieva, T. Tabakova, G. Pantaleo, I. Ivanov, R. Zanella, D. Paneva, N. Velinov, J. W. Sobczak, W. Lisowski, G. Avdeev and A. M. Venezia, *Appl. Catal. A-Gen.*, 2013, **467**, 76-90.
12. T. R. Reina, S. Ivanova, V. Idakiev, J. J. Delgado, I. Ivanov, T. Tabakova, M. A. Centeno and J. A. Odriozola, *Catal. Sci. Tech.*, 2013, **3**, 779-787.
13. T. R. Reina, A. A. Moreno, S. Ivanova, J. A. Odriozola and M. A. Centeno, *ChemCatChem*, 2012, **4**, 512-520.
14. A. Alvarez, S. Ivanova, M. A. Centeno and J. A. Odriozola, *Appl. Catal. a-Gen.*, 2012, **431**, 9-17.
15. X. W. Xie, Y. Li, Z. Q. Liu, M. Haruta and W. J. Shen, *Nature*, 2009, **458**, 746-749.
16. Y. Liu, B. C. Liu, Q. Wang, C. Y. Li, W. T. Hu, Y. X. Liu, P. Jing, W. Z. Zhao and J. Zhang, *J. Catal.*, 2012, **296**, 65-76.
17. B. C. Liu, Y. Liu, C. Y. Li, W. T. Hu, P. Jing, Q. Wang and J. Zhang, *Appl. Catal. B-Env.*, 2012, **127**, 47-58.
18. L. Ilieva, P. Petrova, T. Tabakova, R. Zanella, M. V. Abrashev, J. W. Sobczak, W. Lisowski, Z. Kaszkur and D. Andreeva, *Catal. Today*, 2012, **187**, 30-38.
19. T. Tabakova, D. Dimitrov, M. Manzoli, F. Vindigni, P. Petrova, L. Ilieva, R. Zanella and K. Ivanov, *Catal. Comm.*, 2013, **35**, 51-58.
20. H. J. Freund, *Ang. Chem.-Int. Ed.*, 1997, **36**, 452-475.
21. S. Bordiga, E. Groppo, G. Agostini, J. A. van Bokhoven and C. Lamberti, *Chem. Rev.*, 2013, **113**, 1736-1850.
22. C. Garino, E. Borfecchia, R. Gobetto, J. A. van Bokhoven and C. Lamberti, *Coord. Chem. Rev.*, 2014, **277**, 130-186.
23. J. A. van Bokhoven and C. Lamberti, in *X-Ray Absorption and X-Ray Emission Spectroscopy: Theory and Applications* eds. J. A. van Bokhoven and C. Lamberti, Eds., John Wiley & Sons Ltd, Hoboken, NJ, 2016, vol. 2, ch. 13, pp. 353-383.
24. A. I. Frenkel, *Chem. Soc. Rev.*, 2012, **41**, 8163-8178.
25. A. I. Frenkel, C. W. Hills and R. G. Nuzzo, *J. Phys. Chem. B*, 2001, **105**, 12689-12703.
26. C. Lamberti, E. Groppo, G. Spoto, S. Bordiga and A. Zecchina, *Adv. Catal.*, 2007, **51**, 1-74.
27. A. Vimont, F. Thibault-Starzyk and M. Daturi, *Chem. Soc. Rev.*, 2010, **39**, 4928-4950.
28. C. Lamberti, A. Zecchina, E. Groppo and S. Bordiga, *Chem. Soc. Rev.*, 2010, **39**, 4951-5001.
29. S. Bordiga, C. Lamberti, F. Bonino, A. Travert and F. Thibault-Starzyk, *Chem. Soc. Rev.*, 2015, **44**, 7262-7341.
30. M. Manzoli and F. Vindigni, in *Gold Catalysis*, eds. L. Prati and A. Villa, Eds., Pan Stanford Publishing Pte. Ltd., Singapore, 2016, ch. 8, pp. 205-252.
31. O. Mathon, A. Beteva, J. Borrel, D. Bugnazet, S. Gatla, R. Hino, I. Kantor, T. Mairs, M. Munoz, S. Pasternak, F. Perrin and S. Pascarelli, *J. Synchrotron Rad.*, 2015, **22**, 1548-1554.
32. M. Newville, *J. Synchrotron Rad.*, 2001, **8**, 96-100.
33. S. J. A. Figueroa, D. Gibson, T. Mairs, S. Pasternak, M. A. Newton, M. Di Michiel, J. Andrieux, K. C. Christoforidis, A. Iglesias-Juez, M. Fernandez-Garcia and C. Prestipino, *J. Appl. Cryst.*, 2013, **46**, 1523-1527.
34. S. Scire, P. M. Riccobene and C. Crisafulli, *Appl. Catal. B-Env.*, 2010, **101**, 109-117.
35. S. Ivanova, V. Pitchon, C. Petit and V. Caps, *ChemCatChem*, 2010, **2**, 556-563.
36. I. Castellanos, P. Bazin, S. Thomas, O. Marie and M. Daturi, *Top. Catal.*, 2016, **59**, 337-346.
37. F. Boccuzzi, A. Chiorino, M. Manzoli, P. Lu, T. Akita, S. Ichikawa and M. Haruta, *J. Catal.*, 2001, **202**, 256-267.
38. M. Manzoli, F. Boccuzzi, A. Chiorino, F. Vindigni, W. Deng and M. Flytzani-Stephanopoulos, *J. Catal.*, 2007, **245**, 308-315.
39. X. Wu, L. Senapati, S. K. Nayak, A. Selloni and M. Hajaligol, *J. Chem. Phys.*, 2002, **117**, 4010-4015.
40. A. Fielicke, G. von Helden, G. Meijer, D. B. Pedersen, B. Simard and D. M. Rayner, *J. Am. Chem. Soc.*, 2005, **127**, 8416-8423.
41. A. Badri, C. Binet and J. C. Lavalley, *J. Chem. Soc.-Faraday Trans.*, 1997, **93**, 2121-2124.
42. C. Binet and M. Daturi, *Catal. Today*, 2001, **70**, 155-167.
43. C. Binet, M. Daturi and J. C. Lavalley, *Catal. Today*, 1999, **50**, 207-225.
44. B. P. C. Hereijgers, T. M. Eggenhuisen, K. P. de Jong, H. Talsma, A. M. J. van der Eerden, A. M. Beale and B. M. Weckhuysen, *J. Phys. Chem. C*, 2011, **115**, 15545-15554.
45. J. T. Miller, A. J. Kropf, Y. Zha, J. R. Regalbuto, L. Delannoy, C. Louis, E. Bus and J. A. van Bokhoven, *J. Catal.*, 2006, **240**, 222-234.
46. N. Weiher, E. Bus, L. Delannoy, C. Louis, D. E. Ramaker, J. T. Miller and J. A. van Bokhoven, *J. Catal.*, 2006, **240**, 100-107.
47. G. Agostini, A. Piovano, L. Bertinetti, R. Pellegrini, G. Leofanti, E. Groppo and C. Lamberti, *J. Phys. Chem. C*, 2014, **118**, 4085-4094.
48. G. Agostini, R. Pellegrini, G. Leofanti, L. Bertinetti, S. Bertarione, E. Groppo, A. Zecchina and C. Lamberti, *J. Phys. Chem. C*, 2009, **113**, 10485-10492.
49. C. Lamberti, S. Bordiga, D. Arduino, A. Zecchina, F. Geobaldo, G. Spano, F. Genoni, G. Petrini, A. Carati, F. Villain and G. Vlaic, *J. Phys. Chem. B*, 1998, **102**, 6382-6390.
50. W. Deng, A. I. Frenkel, R. Si and M. Flytzani-Stephanopoulos, *J. Phys. Chem. C*, 2008, **112**, 12834-12840.
51. K. I. Hadjiivanov and G. N. Vayssilov, *Adv. Catal.*, 2002, **47**, 307-511.

ARTICLE

Journal Name

52. E. Garrone, B. Bonelli, C. Lamberti, B. Civalieri, M. Rocchia, P. Roy and C. O. Arian, *J. Chem. Phys.*, 2002, **117**, 10274-10282.
53. T. Tabakova, M. Manzoli, F. Vindigni, V. Idakiev and F. Boccuzzi, *J. Phys. Chem. A*, 2010, **114**, 3909-3915.

